*Journal of Modern Optics*
Vol. 52, No. 7, 10 May 2005, 1019–1030

Taylor & Francis
Taylor & Francis Group

# Hole-assisted energy deposition in dielectrics and clusters in the multiphoton regime[1]

L. N. GAIER*†, M. LEIN‡, M. I. STOCKMAN§, G. L. YUDIN¶, P. B. CORKUM¶, M. YU. IVANOV¶ and P. L. KNIGHT†

†Quantum Optics and Laser Science, Blackett Laboratory, Imperial College London, Prince Consort Road, London SW7 2BW, UK
‡Max Planck Institute for the Physics of Complex Systems, Nöthnitzer Straße 38, D-01187 Dresden, Germany
§Department of Physics and Astronomy, Georgia State University, Atlanta, GA 30303, USA
¶Femtosecond Science Program, Steacie Institute for Molecular Sciences, National Research Council of Canada, 100 Sussex Drive, Ottawa, ON, K1A 0R6, Canada

(*Received 15 November 2004; in final form 27 January 2005*)

We propose a novel mechanism of energy absorption in dielectric materials with ultrashort infrared laser pulses of intensities below the damage threshold. Analytical theory, generalized to hole-assisted processes in arbitrarily polarized laser fields, is validated using one-dimensional numerical simulations of the time-dependent Schrödinger equation. Large enhancements in the multiphoton transition rates are found both numerically and analytically. The one-dimensional calculations are extended to two dimensions via a forest fire percolation model, in which nanoplasma-like structures have been identified.

## 1. Introduction

Laser-induced breakdown (LIB) within dielectrics has been the subject of extensive research ever since the advent of high-power laser systems. Its benefits and uses are numerous (see [1] and references therein), including micromachining, micro-optics [2], ophthalmic surgery, electronics production, data storage, plasma mirrors, transmission gratings [3, 4] and waveguides [5, 6]. LIB is also, however, a severe restriction on laser system performance because of the damage that it causes in optical components.

Extensive research has been carried out in this field, for pulse durations ranging from nanoseconds to femtoseconds in the infrared (IR) regime (see, for example, [7–9]) and is still ongoing. Virtually all research has concentrated on surface effects

[1]Reviewing of this paper was handled by a member of the Editorial Board.
*Corresponding author. Email: lucien.gaier@imperial.ac.uk

*Journal of Modern Optics*
ISSN 0950–0340 print/ISSN 1362–3044 online © 2005 Taylor & Francis Group Ltd
http://www.tandf.co.uk/journals
DOI: 10.1080/09500340500067174

and phenomena, thus avoiding the difficulty of interpretation associated with nonlinear propagation effects in the material [10]. Much is already understood in the field, with the following three-stage process being widely accepted as the central physical mechanisms behind LIB [11, 12].

(i) Seed electrons in the material, made up initially of background conduction-band electrons (CBE), are significantly increased in number via conventional photoionization channels (primarily multiphoton ionization (MPI)).
(ii) Heating of the free electrons occurs via inverse Bremsstrahlung in the laser field, as a result of multiple laser-assisted collisions with the material lattice. This is generally accompanied by a decline in the CBE population due to recombination and diffusion.
(iii) High-energy electrons, with energies exceeding the band gap, can collisionally promote more bound electrons into the conduction band. With sufficient electron density, this will lead to avalanche ionization (AVI) in the material. The transfer of electron plasma energy to the material lattice structure is responsible for the damage to the media.

Further information on the generation of lattice defects through relaxation of electrons and holes generated during the laser pulse can be found in [10]. In the traditional scheme, the mechanisms and damage morphology of LIB have been found to be strongly dependent on the temporal laser pulse width $\tau$, and the laser fluence (defined as the time integral of the laser intensity over the temporal pulse duration) required to promote damage within the material scales with $\tau^{1/2}$. This scaling law was predicted via the Drude model for the ac-conductivity in metals, and has been experimentally verified (see [13] and references therein).

This article will begin with a brief review of the physics behind LIB and will discuss the relevance of our work to this subject. It will then proceed to discuss new physical processes behind LIB in the ultrashort-IR laser pulse regime and will conclude by discussing future directions of our work.

### 1.1 *Long pulse durations ($\tau > 10$ ps)*

The actual physical damage caused by the laser interaction is attributed to the transfer of plasma energy to the lattice [7, 8, 14]. When the laser pulse interacts with the material, the background CBEs within the material are heated by the incoming radiation, which then collisionally excite valence electrons into the conduction band. CBEs will most efficiently excite valence electrons when their energy exceeds that of the band gap $I_P$ by a factor of 2–3. The free-electron density within the material is therefore increased from about $10^{10}\,\mathrm{cm}^{-3}$ to about $10^{21}\,\mathrm{cm}^{-3}$.

The free-electron density is now of the order of the critical plasma density, and the material becomes highly absorbing or opaque to the incoming laser energy, which is generally accepted as being the point at which LIB occurs. In these long pulse durations, the damage itself occurs over the entire area irradiated, resulting in melting and boiling of the material. The damage occurs both during and just after the pulse has passed, as plasma energy is transferred to the lattice structure.

### 1.2 *Short pulse durations ($\tau < 10$ ps)*

As the pulse durations shorten, the damage morphology changes and becomes more deterministic (and, hence, practically more useful) [12, 13, 15, 16]. When the

pulse is focused on to the surface of the dielectric, the material suffers primarily from surface ablation, the formation of lattice defects, and small volume melting, all occurring with little collateral damage. The damage occurs at the peak of the Gaussian irradiance profile, within an area up to $10^6$ smaller than the spot size. Bulk-material effects have recently begun to be investigated in depth [17]. In [1], for instance, there is a description of permanent bulk damage to be characterized by a damage zone, generally a few tens of microns in diameter, followed by a long filamentary track, extending up to 80 μm from the first damage zone.

Generation of CBEs through MPI at the peak of the laser pulse dominates over the number of free background electrons. Additionally, the short timescale of the interaction 'freezes' out the heat diffusion process. Hence the plasma formation is highly localized at the laser focus site, and the LIB occurs with less statistical uncertainty.

### 1.3 *Ultrashort pulse durations ($\tau < 50$ fs)*

The physics of the energy deposition in the material will inevitably change when few-cycle low-frequency laser pulses are considered. Taken as an example case, a laser intensity $I \approx 10^{13}$ W cm$^{-2}$ and a wavelength $\lambda = 800$ nm result in a ponderomotive energy $U_P = 0.6$ eV given by

$$U_P = \frac{e^2 E^2}{4m\omega^2}, \tag{1}$$

where $e$ is electronic charge, $E$ the momentary electric field of the incident laser, $m$ the electronic mass and $\omega$ the angular frequency of the field. MPI occurs near the peak of laser pulse and so, for the remainder of the pulse, CBEs absorb approximately $2U_P$ per collision per laser half-cycle each (given that collisions do not occur more than once per laser half-cycle). The energy absorption occurs through the laser-driven motion of the dipole moment that exists between the ionized parts of the electronic wave function and the bound parts near the atomic core. When the ionized part is driven back in close proximity to the core, energy is imparted to the electronic centre of mass. Neglecting any energy loss, we see that for fused silica ($SiO_2$) (band-gap energy, 9 eV) the minimum time taken to absorb 10–20 eV will be 15–25 fs; this gives an avalanche timescale of around 30–50 fs. This is roughly the pulse duration at which the traditional AVI mechanisms begin to appear.

Therefore, even under optimal conditions of zero energy loss and well-timed collisions, a 10 fs pulse is *too short* for conventional avalanche mechanisms to develop. The question is: how is it possible for a catastrophic increase in carrier density to occur within less than 30 fs without the traditional heating mechanisms?

Two new physical mechanisms have been proposed which allow an avalanche in carrier density to develop within these ultrashort timescales [18, 19] and require little or no heating of the CBEs. Both processes are dependent on the concentration of charge carriers (electrons or ion holes) and hence will develop like an avalanche. The effect dependent on the hole concentration within the material will be discussed here. The analytic solutions to these effects are provided within the framework of Keldysh's strong-field approximation (SFA) [20], which can then be directly compared with numerical simulations.

## 2. Hole-assisted multiphoton ionization forest fires

The proximity of a positive potential well (such as an ion, dopant or lattice defect) modifies the local potential seen by a bound electron. The binding energy of the electron is reduced and the tunnelling probability is exponentially increased as a result. The mechanism is similar to enhanced ionization in molecules [21, 22]. For clusters, this process has also been studied in the high-intensity regime of multiply charged ion formations, ionization ignition [23] and Coulomb explosions [24]. However, we shall restrict ourselves to significantly lower intensities.

The physical theory is as follows. When an electron is promoted to the conduction band, it leaves in its place a much heavier, positively charged hole. The electron is removed from the vicinity of the hole within the next laser cycle, while the remaining heavier potential well is considered fixed in place. Neighbouring systems will feel the combined effects of the laser field $\boldsymbol{E}_{\mathrm{F}} = \boldsymbol{E}\cos(\omega t)$ and the hole $\boldsymbol{E}_{\mathrm{h}} = \boldsymbol{D}/D^3$, where $\boldsymbol{D}$ is the radius vector to the hole. It should be noted that solutions using SFA theory require the neighbouring potential well to be approximated by a homogeneous dc-field, rather than by a Coulombic potential. This is most applicable when there is a large atom–ion separation distance $D$. As for the SFA itself, it is reliable when $\gamma^2 = I_{\mathrm{P}}/2U_{\mathrm{P}} < 1$, where $\gamma$ is Keldysh's gamma factor.

The analytical theory is general and, as such, is applicable to any laser polarization or hole–ion geometry, although it is insightful first to look at the simplest case scenario. Reducing the problem to one dimension, the laser is assumed to be linearly polarized and dipole approximated: $\boldsymbol{E}\cos(\omega t)$; the electric field of the hole is given by $1/D^2$. The additional electric field leads to barrier suppression at the adjacent molecular sites, which exponentially enhances the transition rate at these sites (see figure 1). An example of the modifications employed in the SFA theory can be seen in the tunnelling regime $\gamma^2 \ll 1$, where the quasistatic tunnelling rate [24]

$$\Gamma_{\mathrm{qs}}(t) \propto \exp\left(-\frac{2(2I_{\mathrm{P}})^{3/2}}{3|\boldsymbol{E}\cos(\omega t)|}\right) \tag{2}$$

is modified by adding the static field of the positive hole, $|\boldsymbol{E}\cos(\omega t)| \rightarrow |\boldsymbol{E}\cos(\omega t) + \boldsymbol{E}_{\mathrm{h}}|$. The detailed description of the analytical model can be found in [18].

The creation of ions at adjacent lattice sites to the hole is therefore exponentially increased, acting as nucleation sites similar to that in forest fire or percolation models. This encourages the formation of ionization regions, each of which expand along their boundary. As an ionization region grows, the role of the original ions far removed from its perimeter is diminished.

The enhancement in ionization rate promotes the accelerated creation of holes. As the effect is proportional to hole density, ionization will therefore develop in an avalanche-like manner. The mechanism described here involves multiphoton transitions and, as such, are inherently weak compared with collisional excitation of electrons across the band gap. However, as the timescale of the interaction precludes the development of the traditional LIB mechanisms, these new processes should become dominant.

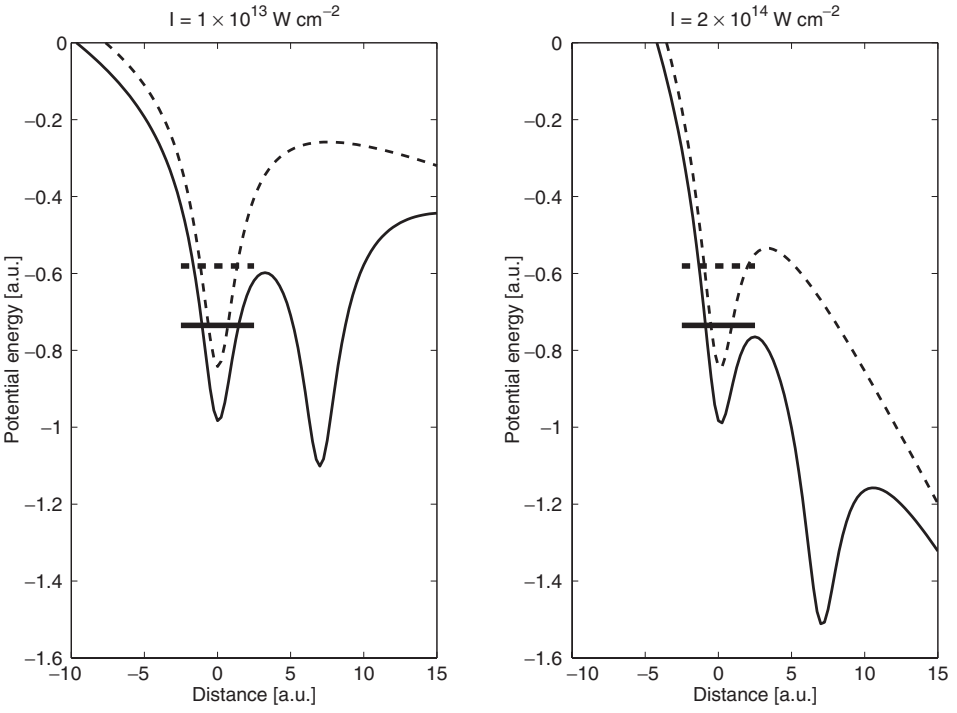


Figure 1. Atomic potentials representing the argon system, with (solid curves) and without (dashed curves) the hole ($D = 7$ au) at two different laser intensities. Ground-state energies of the parent atom are shown by the respective horizontal bars.

## 3. Numerical modelling

The next step is to compare the general analytical theory with numerical simulations. The numerical model is a one-dimensional grid with absorbing boundaries with a soft-core potential depicting the atom site located at its centre (considered to be $x = 0$). Within this first well sits the ground-state wave packet of an electron. The ground-state energy of 9 eV for $SiO_2$, for instance, can be reproduced using a soft-core parameter $\epsilon = 5.2$ in a regularized potential

$$V = -\frac{1}{(x^2 + \epsilon)^{1/2}}. \tag{3}$$

For the case of argon, the $I_P$ value of 15.76 eV is reproduced using an $\epsilon$ value of 1.41. Note that the results that follow are for the case of argon. This is chosen for numerical convenience, as the deeper potential well allows for the use of smaller numerical grids. The determination of the ground state and the propagation of the wave function is accomplished using the split-operator method (with imaginary time propagation in the case of the ground-state determination) and is carried out within the velocity gauge [25, 26]. The absorbing boundary regions of the grid is set to be one sixteenth of the grid size in total, with a $\sin^2$ mask function within the boundary region that removes spurious reflections from the grid boundaries. The addition of one positive potential hole has so far been attempted. It is a soft-core potential well,

identical with the first, located at a distance $D = 7$ au away (as in figure 1). This distance is chosen as it is approximately the binding distance in large argon clusters.

$$V = -\frac{1}{(x^2+\epsilon)^{1/2}} - \frac{1}{\left[(x-D)^2+\epsilon\right]^{1/2}}. \tag{4}$$

As discussed earlier, the analytical theory assumes the combined system potential to be given by

$$V = -\frac{1}{(x^2+\epsilon)^{1/2}} - \frac{x}{D^2}. \tag{5}$$

Employing this dc-field approximation rather than the full-potential description used in the simulations has been shown to give significantly different ionization enhancement behaviours. This will be discussed further in the next section.

Laser intensities used in the theory and numerics typically range from $I = 10^{12}$ W cm$^{-2}$ to $I = 10^{15}$ W cm$^{-2}$, with a laser wavelength of 800 nm. The most interesting region lies within the range $I \approx 10^{13} - 10^{14}$ W cm$^{-2}$ as it is the region in which the electric fields of the hole and the laser pulse become comparable. Furthermore, it can be seen in figure 1 that, at $I = 2 \times 10^{14}$ W cm$^{-2}$ and above, barrier suppression is observed in the potential from which the electron wave packet is born (and, hence, quasistatic tunnelling solutions are no longer applicable). The pulse shape is trapezoidal, with linear ramping on and off for 2 laser cycles and 16 laser cycles at maximum intensity being used in the results so far.

## 4. Results

To quantify the effect that the proximity of the hole has, the enhancement factor $K$ with respect to ionization rates $\Gamma$ is calculated:

$$K = \frac{\Gamma_1}{\Gamma_0}. \tag{6}$$

The rates $\Gamma_1$ and $\Gamma_0$ (rates with and without the presence of the hole respectively) are calculated as being the rate of change in the total norm of the still-bound sections of the time-dependent wave-packet state $|\psi(t)\rangle$. The time-dependent norms produced by the code are then fitted to the exponential rate equation

$$|\psi(\tau)|^2 = \exp(-\Gamma\tau). \tag{7}$$

This allows the rate $\Gamma$ to be calculated by knowing the final norm at the end of the laser pulse and the pulse duration:

$$\Gamma = -\frac{1}{\tau}\ \ln|\psi(\tau)|^2. \tag{8}$$

To ensure that only bound parts of the wave packet are used, the ground state $|g\rangle$ and first excited states $|e\rangle$ of the two-site system are projected out of $|\psi(\tau)\rangle$. The lowest two states are sufficient as around 99% of the wave packet will remain in these states after 'turning on' the ion site. They are also the two states belonging to the valence band of our two-site dielectric model.

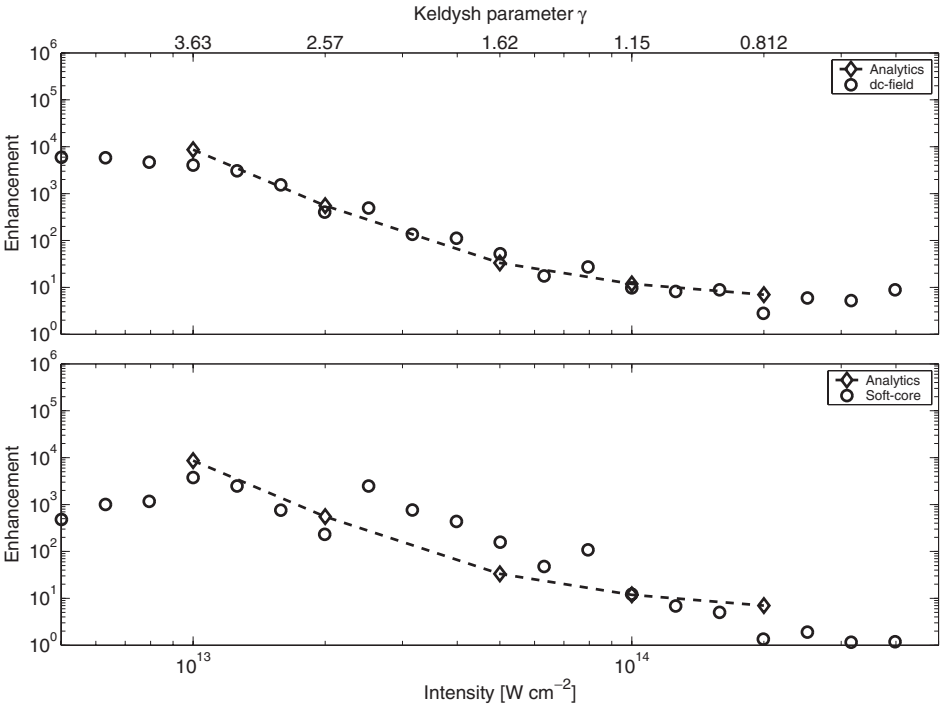


Figure 2. Comparison between $K$ values for argon given by the numerical model (open circles) in relation to the SFA theory (dashed curve). The upper plot gives a comparison where the effective field produced by ion is a homogeneous dc-field. The lower plot has the ion field as a soft-core potential.

Typical enhancement curves can be seen in figure 2. The results for $K$ are plotted as a function of intensity derived analytically and numerically. If the numerical model uses the dc-field approach to describe the influence of the ion, the numerics and the theory very closely resemble each other. With the full-potential description, the presence of additional structures within the numerics indicate that there are additional effects not considered in the theory, such as resonances and population trapping.

An explanation for these effects can be seen in figure 3. This shows the evolution of the electron wave packet in time for both types of combined system potential. In the double soft-core potential type, the electron wave packet can be seen to repeatedly recollide with the double well. This would give rise to more complex structures in the enhancement curves than can be explained by the SFA analytical theory, and most likely the generation of high harmonics from the interaction. The homogeneous dc-field-type system, however, has much simpler ionization dynamics. The majority of the ionization occurs at the peaks in the laser field strength. The asymmetry of the combined well also ensures that the ionization occurs in one direction only. This more clearly resembles the SFA model and, as such, the numerics follow the predictions much more closely. It should also be noted that there is good quantitative agreement even for relatively high $\gamma$ values, a regime in which tunnelling theory tends to break down. This surprising agreement has been explained in [19].

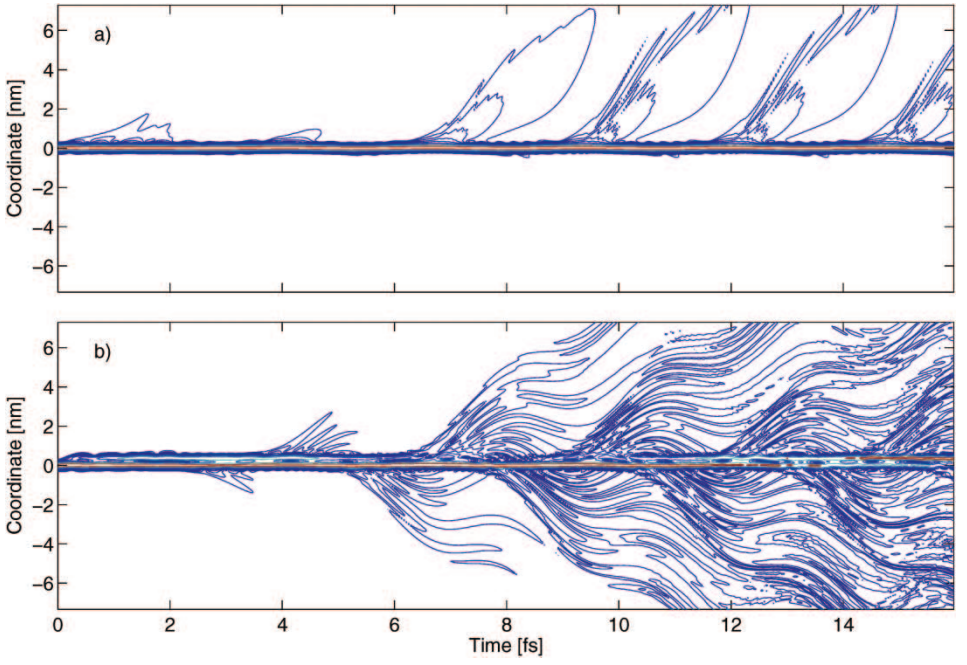


Figure 3. Evolution of the total electronic wave packet during the first 16 fs of the trapezoidal laser pulse ($I = 5 \times 10^{13}$ W cm$^{-2}$; other parameters as given in the text) for (*a*) soft-core plus dc-field ion and (*b*) double soft-core potential wells description. The electron's parent atom is situated at the centre, and the ion is situated a distance $D = 7$ au (0.37 nm) in the positive coordinate direction. Contours represent the levels of probability density, ranging from unity down to $10^{-4}$ in ten logarithmic steps.

## 5. Application to clusters: forest fires

In order to apply the model better to macroscopic media, it is necessary to remove the one-dimensional approximations, which can easily be done analytically. The one-dimensional ionization rates obtained above can be extrapolated to predict the ionization behaviour of a macroscopic two-dimensional sample of sites, as long as the laser polarization remains linear. This can be achieved by determining the enhancement due to the ionization of a number of nearest-neighbour sites. Their number, relative geometry, and orientation with respect to the laser field (figure 4) are critical factors in determining the enhancement factors $K_{i,k}$, where $i$ and $k$ represent the site indices. The expansion of the ionized regions is modelled by the stochastic finite-difference equation

$$\Delta P_{i,k} = \Gamma_0 K_{i,k} p_{i,k} \Delta t, \tag{9}$$

where $\Delta P_{i,k}$ is the ionization probability of the site with indices $i, k$ during the time step $\Delta t$. The factor $p_{i,k}$ takes only two values, 0 or 1; $p_{i,k} = 1$ indicates that the site is neutral at the beginning of this time step, and $p_{i,k} = 0$ that it is ionized. The value of $K_{i,k}$ is obtained at each time step from a look-up table, determined using the SFA theory for a large number of site geometries, and is independent of the time step. With no ionized neighbours the value of $K_{i,k}$ is unity. At the end of every time step

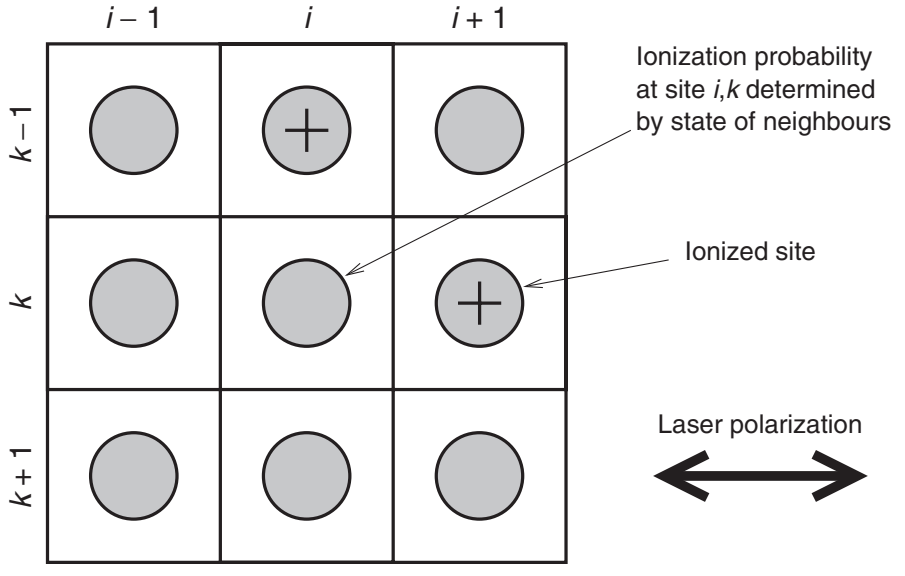


Figure 4. Schematic diagram of the atom site at $i, k$ (with its bound electron) and the eight nearest neighbours on the two-dimensional surface. Each site, if an ion, contributes to $K_{i,k}$, with their orientation with respect to the polarization direction and the character of their nearest neighbours being taken into account.

a random number $r_{i,k}$ between 0 and 1 is generated for each site, and $\Delta P_{i,k}$ is compared with $r_{i,k}$. The site is deemed ionized and $p_{i,k} \to 0$ if $\Delta P_{i,k} > r_{i,k}$, while for $\Delta P_{i,k} < r_{i,k}$ the site remains neutral. If the site is ionized, it enhances the ionization rate for adjacent sites $i' = i \pm 1, k' = k \pm 1$. The value for $\Gamma_0$ is obtained from the numerical simulations.

This is a particular type of model called a 'forest fire' model [27], where the still bound sites are the 'trees', the ionized sites are the burning trees, and the 'lightning strikes' are due to the laser field. Self-organized criticality (SOC) in this particular system is not possible, as the regrowth mechanism required in forest fire models for SOC to occur is absent [28]. The recombination of electrons with ion sites would fulfil this role but the timescale of the interaction is much shorter than typical recombination times (about 150 fs).

A typical picture of the propagation (or percolation) of ionization regions on the surface of the material can be seen in figure 5. Here, it is clear to see that initially there is a favoured growth direction in the percolation structures, determined by the laser polarization direction, and that the level of clustering in these ionization regions is quite high, even with relatively low $K_{i,k}$ values that apply to this intensity ($I = 5 \times 10^{13}$ W cm$^{-2}$). As the ionization degree increases, these structures become more 'round'. These ionization regions will have high local electron–ion densities, structures familiar to researchers in laser–cluster interactions as nanoplasmas [29]. Note that, by neglecting the enhancement effect (set $K_{i,k} = 1$ always), sites reach full ionization at around 6 ps. This is likely to increase if the recombination rate were to be included. It should be noted that, by employing such a simple model, the ionization times are unlikely to be completely accurate. However, the dramatic speed-up in ionization is unquestionable and is robust against changes in the chosen parameters.

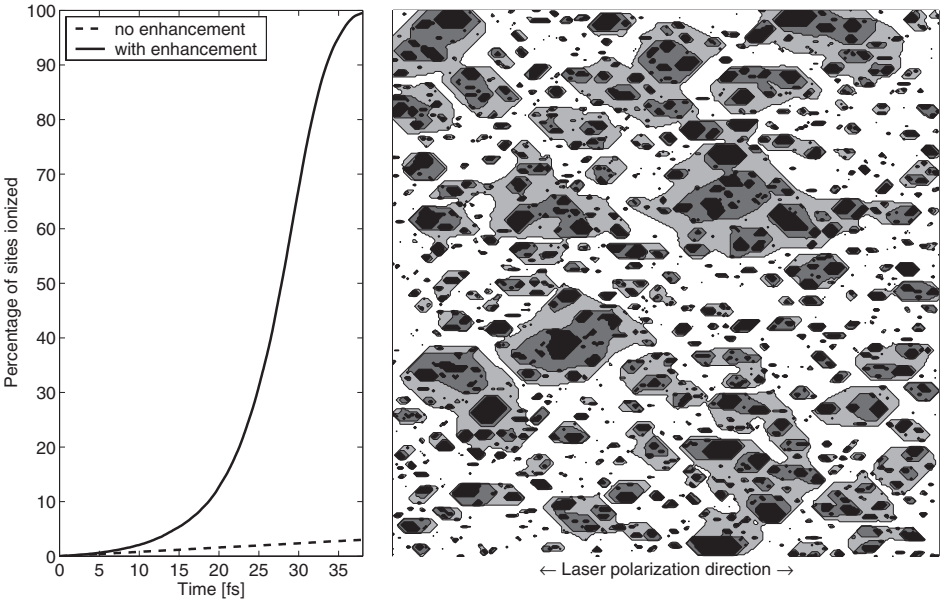


Figure 5. Left-hand plot illustrates the population curve of ionized sites for the two-dimensional model, with and without the enhancement effect. The laser intensity used is $I = 5 \times 10^{13}$ W cm$^{-2}$, giving a $\Gamma_0$ value of $8 \times 10^{11}$ s$^{-1}$. Without the enhancement effect, the sites approach 100% ionized at about 6 ps. To the right, a typical forest fire simulation of a large argon cluster surface at the same intensity, showing 10% ionization (black regions), growing to 25% ionization (dark-grey regions) at a later time, and 50% ionization (light-grey regions) later still. White areas represent sites that are as yet unionized.

In the numerical simulations shown in figure 5, we have used a very simple model to account for collective effects associated with nanoplasmas. We have not taken into account effects associated with excitation of surface plasmons and the corresponding modification of local electric fields near the plasma nanodroplets. Instead, we simply assumed that holes inside the ionized regions are screened and only holes at the surface of the nanodroplets are participating in enhancing the ionization rates at adjacent sites. In practice, modification of local fields near nanoplasma droplets will be different owing to the excitation of surface plasmons. In particular, as the size of the nanoplasma grows, it will start to shield the electric field along the droplet's equator (i.e. along the laser polarization), while enhancing it at the poles. This is likely to change the direction of preferential growth from parallel to laser polarization to perpendicular. This may explain experimental results such as those in [17]. The role of surface plasmons and the dynamic collective response will be considered elsewhere.

## 6. Conclusion

Work so far has provided an insight into the mechanics and the dependences of the hole-assisted MPI process, which we believe plays an important role in the first stages of LIB, particularly for pulses lasting a few tens of femtoseconds or less. The pulse width and shape have turned out to be important system properties

in determining enhancement profiles, properties that are not accounted for in the quasistatic tunnelling rates calculated within Keldysh's SFA theory. Further enhancement to the theory would involve a time-dependent turn-on of the ion site to achieve a more physical model, and self-consistency at the lowest intensities on higher $\gamma$ values. The SFA theory is applicable for any laser ellipticity, orientation of holes, and phase dependence, so it is possible to look at systems with multiple ion sites.

Another important approximation is in the description of the ion site; the dc-field approximation does neglect some effects, such as charge-resonance enhancements. However, it is clear that hole-assisted energy deposition is a significant effect on these timescales, and that good quantitative agreement can be reached between numerics and theory. Efforts are also under way to refine the forest fire model, such as looking at the relative effect of plasma screening on the influence of the ion sites. This would lead to time-dependent $K$ values that will probably change the way in which the percolation structures grow with time. It is also necessary to examine the collision-assisted MPI avalanche scenario, outlined in [18], and the enhancement in ionization that this mechanism provides. Our goal is to combine these effects, to compare them with current experimental data and to provide quantitative predictions for future experiments.

## Acknowledgments

We acknowledge discussions with J. M. Rost, J. Marangos, R. Bhardwaj, D. Rayner and R. Taylor. We are grateful to A. Sarychev and J. Sipe for numerous suggestions and illuminating advice. M. Yu. Ivanov additionally acknowledges stimulating discussions with V. Shalaev. This work was supported in part by the UK Engineering and Physical Sciences Research Council, the Canadian National Research Council and the British Council. The work of M. Stockman is supported by grants from the Chemical Sciences, Biosciences and Geosciences Division of the Office of Basic Energy Sciences, Office of Science, US Department of Energy, and from the US–Israel Binational Science Foundation.

## References

[1] L. Sudrie, A. Couairon, M. Franco, *et al.*, Phy. Rev. Lett. **89** 186th 601 (2002).
[2] E. Bricchi, J.D. Mills, P.G. Kazansky, *et al.*, Optics Lett. **27** 2200 (2002).
[3] E.N. Glezer, M. Milosavljevic, L. Huang, *et al.*, Optics Lett. **21** 2023 (1996).
[4] D. Homoelle, S. Wielandy and A.L. Gaeta, Optics Lett. **24** 1311 (1999).
[5] K.M. Davis, K. Miura, N. Sugimoto and K. Hirao, Optics Lett. **21** 1729 (1996).
[6] K. Miura, H. Inouye, Q. Jianrong, *et al.*, Nucl. Instrum. Meth. B **141** 726 (1998).
[7] B.C. Stuart, M.D. Feit, S. Herman, *et al.*, Phys. Rev. B **53** 1749 (1996).
[8] D. Du, X. Liu, G. Korn, *et al.*, Appl. Phys. Lett. **64** 23 (1994).
[9] I.M. Azzouz, J. Phys. B: At. Molec. Opt. Phys. **37** 3259 (2004).
[10] S.S. Mao, F. Quéré, S. Guizard, *et al.*, Appl. Phys. A **79** 1695 (2004).
[11] D. Arnold and E. Cartier, Phys. Rev. B **46** 15th 102 (1992).
[12] An-C. Tien, S. Backus, H. Kapteyn, *et al.*, Phys. Rev. Lett. **82** 3883 (1999).
[13] T. Apostolova and Y. Hahn, J. Appl. Phys. **88** 1024 (2000).
[14] B. Stuart, M. Feit, A. Rubenchik, *et al.*, Phys. Rev. Lett. **74** 2248 (1995).
[15] M. Lenzner, J. Krüger, S. Sartania, *et al.*, Phys. Rev. Lett. **80** 4076 (1998).

[16] T.Q. Jia, R.X. Li, Z. Liu, *et al.*, Appl. Surf. Sci. **189** 78 (2002).
[17] J.D. Mills, P.G. Kazansky, E. Bricchi and J.J. Baumberg, Appl. Phys. Lett. **81** 196 (2002).
[18] G.L. Yudin, L.N. Gaier, M. Lein, *et al.*, Laser Phys. **14** 51 (2004).
[19] L.N. Gaier, M. Lein, M.I. Stockman, *et al.*, J. Phys. B: At. Molec. Opt. Phys. **37** L57 (2004).
[20] M. Yu. Ivanov, T. Brabec and N. Burnett, Phys. Rev. A **54** 742 (1996).
[21] T. Seideman, M. Yu. Ivanov and P.B. Corkum, Phys. Rev. Lett. **75** 2819 (1995).
[22] T. Zuo and A.D. Bandrauk, Phys. Rev. A **52** R2511 (1995).
[23] C. Rose-Petruck, K.J. Schafer, K.R. Wilson and C.P.J. Barty, Phys. Rev. A **55** 1182 (1997).
[24] P.B. Corkum, M. Yu. Ivanov and J.S. Wright, An. Rev. Phys. Chem. **48** 387 (1997).
[25] M.D. Feit, J.A. Fleck and A. Steiger, J. Comput. Phys. **47** 412 (1982).
[26] M. Lein, Atoms and molecules in strong laser fields: double ionisation, dissociative ionisation, and harmonic generation. PhD thesis, University of Würzburg, 2001.
[27] P. Fröjdh and M. den Nijs, Phys. Rev. Lett. **78** 1850 (1997).
[28] B. Drossel and F. Schwabl, Phys. Rev. Lett. **69** 1629 (1992).
[29] T. Ditmire, T. Donnelly, A.M. Rubenchik, *et al.*, Phys. Rev. A **53** 3379 (1996).